Accepted Manuscript

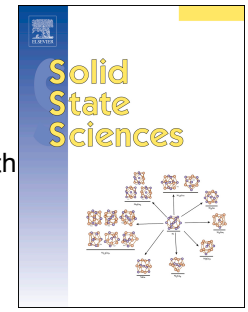

Mechanochemical synthesis, structure and properties of lead containing alkaline earth metal fluoride solid solutions $M_xPb_{1-x}F_2$ (M = Ca, Sr, Ba)

M. Heise, G. Scholz, A. Düvel, P. Heitjans, E. Kemnitz

PII: S1293-2558(17)31099-3

DOI: 10.1016/j.solidstatesciences.2018.01.007

Reference: SSSCIE 5622

To appear in: *Solid State Sciences*

Received Date: 13 November 2017

Revised Date: 5 January 2018

Accepted Date: 16 January 2018

Please cite this article as: M. Heise, G. Scholz, A. Düvel, P. Heitjans, E. Kemnitz, Mechanochemical synthesis, structure and properties of lead containing alkaline earth metal fluoride solid solutions $M_xPb_{1-x}F_2$ (M = Ca, Sr, Ba), *Solid State Sciences* (2018), doi: 10.1016/j.solidstatesciences.2018.01.007.

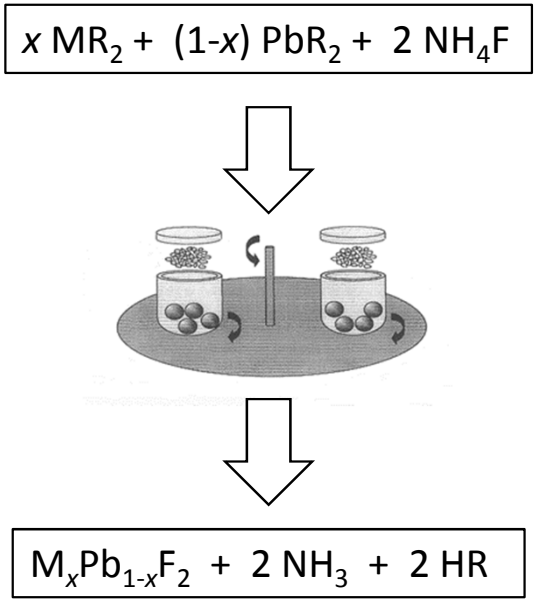
x MR2 + (1-x) PbR2 + 2 NH4F
MxPb1-xF2 + 2 NH3 + 2 HR

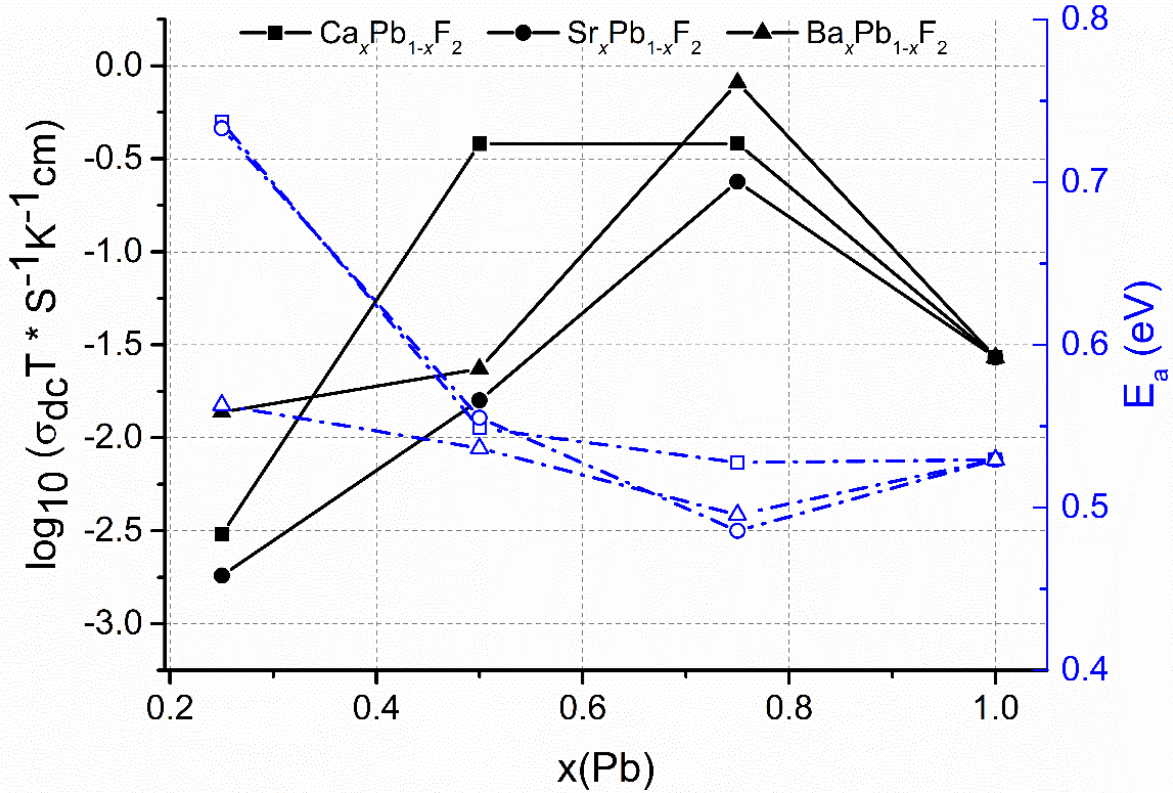
CaxPb1-xF2
SrxPb1-xF2
BaxPb1-xF2
log10 (σdcT * S-1K-1cm)
Ea (eV)
x(Pb)
0.0
-0.5
-1.0
-1.5
-2.0
-2.5
-3.0
0.2
0.4
0.6
0.8
1.0
0.8
0.7
0.6
0.5
0.4

Mechanochemical Synthesis, Structure and Properties of Lead Containing Alkaline Earth Metal Fluoride Solid Solutions $M_xPb_{1-x}F_2$ (M = Ca, Sr, Ba)

M. Heise[a], G. Scholz[a*], A. Düvel[b], P. Heitjans[b], E. Kemnitz[a*]

[a] Humboldt-Universität zu Berlin, Department of Chemistry, Brook-Taylor-Str. 2, D-12489 Berlin, Germany

[b] Leibniz Universität Hannover, Institute of Physical Chemistry and Electrochemistry, ZFM - Center for Solid State Chemistry and New Materials, Callinstr. 3a, D-30167 Hannover, Germany

Corresponding authors:

[*] PD Dr. G. Scholz, email: *Gudrun.Scholz@rz.hu-berlin.de*,

[*] Prof. Dr. E. Kemnitz, email: *erhard.kemnitz@chemie.hu-berlin.de*,

Keywords:

Mechanochemical synthesis, solid solutions, ^{19}F MAS NMR spectroscopy, impedance spectroscopy

Abstract

The paper deals with the mechanochemical synthesis of lead containing alkaline earth metal fluoride solid solutions $M_xPb_{1-x}F_2$ (M = Ca, Sr, Ba) by high-energy ball milling. Several metal precursors and fluorinating agents were tested for synthesizing $M_{0.5}Pb_{0.5}F_2$. Metal acetates and ammonium fluoride as precursors show the most promising results and were therefore used for the formation of $M_xPb_{1-x}F_2$ with different metal cationic ratios. The characterization of the local fluorine coordination and the crystal structure was performed by ^{19}F MAS NMR spectroscopy and X-ray diffraction. Additional calculations of ^{19}F chemical shifts using the superposition model allows a deeper insight into the local structure of the compounds. The fluoride ion conductivity was followed by temperature dependent DC conductivity measurements. Significantly higher conductivities were found in comparison with those of the corresponding binary fluorides. The highest values were be observed for samples with high lead content $M_{0.25}Pb_{0.75}F_2$, bearing in mind the much higher conductivity of PbF_2 compared to MF_2.

Introduction

In search of more efficient energy capacitors or batteries, solid solutions, especially those containing fluorides crystallizing in the fluorite structure, gain raising interest as possible components in fast fluoride ion conductors [1–4]. Distortions of the local fluoride ion environment by the mutual substitutions of cations while keeping the original crystal structure intact lowers the activation energy for the movement of the fluoride ions [5]. This leads to an increasing ionic conductivity making these compounds potentially applicable as solid electrolytes. The application of such systems however, is not only restricted to electric devices. Replacing one cation with, e.g., a rare earth metal ion allows the preparation of compounds with widely spread use in optics [6–11].

A fast and easy approach to synthesize such systems is the mechanochemical reaction. This branch of synthetic chemistry has got increasing attention during the past years for solid state syntheses [12–14]. While the mechanisms of such reactions can be different and are not completely clear yet, a lot of applications have been developed for this method. It is possible to induce phase transformations of compounds, to modify their surfaces and to enhance their catalytic properties[15]. Non-stoichiometric and/or non- equilibrium products like solid solutions [16–18], co-crystals[19,20] and MOFs[21] can be obtained which are more difficult or excluded to get by common synthesis methods like precipitation or thermally induced

reactions. Furthermore, the possibility to avoid using solvents makes mechanochemistry environmentally benign compared to, e.g., the sol-gel-synthesis and may simplify the purification process.

Based on work of Scholz *et al.* [22,23] we showed in 2016 that it is possible to synthesize $M^a_xM^b_{1-x}F_2$ (M = Ca, Sr, Ba) solid solutions by high energy ball milling [17]. By milling a mixture of metal acetates or hydroxides with ammonium fluoride a mutual substitution of cations over all molar ratios is possible for the Ca/Sr and the Ba/Sr systems. For $Ba_xCa_{1-x}F_2$, the formation of solid solutions was observed only with $x > 0.9$ or $x < 0.1$, which may be caused by the size differences of the cations. Conductivity measurements of these systems show significantly increased conductivity values compared to the pure binary fluorides. Similar results could be obtained by Heitjans and co-workers [5,16]. Applying an alternative mechanochemical route, namely milling the pure binary fluorides for long durations (up to 99 hours), they were able to synthesize even $Ba_xCa_{1-x}F_2$, although their system is not stable for long times (more than two years) or at elevated temperatures (above 700 K) [5,16]. However here [5,16], the mutual substitution of cations has a positive effect on ionic conductivity.

While mechanochemical synthesis routes have been established for the alkaline earth metal fluorides only little is known for PbF_2. Until 2016, only one mechanochemical synthesis was described in the literature. Subirana-Manzanares *et al.* [24] published the synthesis of PbF_2 by grinding lead acetate with ammonium fluoride obtaining a paste like compound containing α- and β-PbF_2. Moreover, they were able to direct the formation of either phase by adding organic acids or amines during the reaction. Recently we reported the synthesis of PbF_2 by ball milling different lead precursors with ammonium fluoride [25]. The lead precursor itself determined the formation of the respective PbF_2 phase. The use of lead acetate led to β-PbF_2 (cubic fluorite structure), using lead(II) oxide resulted in mostly α-PbF_2 (orthorhombic structure), and using $PbCO_3$ resulted in a mixture of both phases. As it is beneficial for the formation of solid solutions that both separated binary fluorides crystallize in the same structure, we decided to use for the synthesis of $M_xPb_{1-x}F_2$ (M = Ca, Sr, Ba) the alkaline earth metal acetates and hydroxides as well as lead acetate and carbonate. All described samples were investigated by X-ray powder diffraction (XRD) and magic angle spinning nuclear magnetic resonance (MAS NMR) spectroscopy and for selected samples impedance spectroscopy measurements were carried out.

Experimental section

Preparation: All not self-synthesized starting materials were used as commercially purchased (Table 1). The alkaline earth metal fluorides CaF_2, SrF_2 and BaF_2 were synthesized by ball milling (Fritsch Pulverisette 7, premium line) the corresponding metal hydroxides with ammonium fluoride for four hours at 600 rpm. β-PbF_2 with cubic fluorite structure was prepared by heating a mixture of lead acetate trihydrate and ammonium fluoride in a furnace (Eurotherm, Carbolite RHF 16/3) for two hours at 400 °C (heating rate: 10 K/min).

The syntheses of $M_xPb_{1-x}F_2$ samples were carried out by ball milling the reactants (m = 1 g, ball : powder ≈ 15 g : 1 g; five balls with 12 mm in diameter) for four to eight hours at 600 rpm in silicon nitride beakers (v = 45 ml) according to Scheme 1.

All samples were dried in a furnace for two hours at 160 °C after reaction if not otherwise stated.

XRD*:* X-ray powder diffractograms were measured with an XRD-3003 TT diffractometer (*Seifert*) in the Bragg-Brentano geometry with a range of 2Θ from 5° to 65°. In both cases a CuKα X-ray source (λ = 1.542 Å) was used. The reflections were compared with the JCSPDS-PDF database [26]. Due to the nanocrystalline character of the samples obtained after milling the XRD patterns show typically less intense and broadened reflections. Following that the signal to noise ratio is worse compared to that of crystalline binary fluorides applying the same measurement conditions.

^{19}F MAS NMR: A Bruker AVANCE 400 spectrometer equipped with a 2.5 mm magic angle spinning (MAS) probe (Bruker Biospin) was used to record ^{19}F MAS NMR spectra (Larmor frequency: ν_{19F} = 376.4 MHz). All spectra were registered using a π/2 pulse length of 4 µs, a spectrum width of 400 kHz, a recycle delay of 5 s, an accumulation number of 64, and a rotation frequency of 20 kHz. Recycle delays longer than 5 s were tested to ensure the completeness of the signals and to inspect their spin-lattice relaxation behavior. All isotropic chemical shift values of ^{19}F resonances are given with respect to the $CFCl_3$ standard. Existent background signals were suppressed with the application of a phase-cycled depth pulse sequence according to Cory and Ritchey [27]. The rotor-synchronized spin-echo experiments were registered with a recycle delay of 5 s, an accumulation number of 128 and a dipolar evolution time of 0.5 ms. ^{19}F MAS NMR spectra were simulated using the DMFIT program [28].

DC conductivity: The conductivity measurements were performed with pellets of 8 mm in diameter and approximately 1 mm in thickness (measured with a Vernier caliper for each pellet). These were obtained from powders by cold pressing, applying a pressure of approximately 800 MPa. Electrodes were applied by coating the pellets with an alcohol based graphite conductive adhesive (Alfa Aesar). DC conductivities were taken from impedance spectra recorded in the frequency range from 0.01 Hz to 10 MHz with a Novocontrol Concept 41 impedance analyzer. The DC conductivity was read out from the frequency independent plateau in the conductivity spectra. The decrease of the conductivity at lower frequencies is caused by the ion blocking electrodes at which the ions accumulate. This decrease also shows that the electronic conductivity is orders of magnitude smaller than the ionic conductivity. Hence, the DC conductivity read out from the conductivity spectra is the ionic conductivity, except for a negligible part caused by electron conduction.

Results and Discussion

Synthesis of $Ca_xPb_{1-x}F_2$:

At first, different metal precursors were tested using a molar Ca : Pb ratio of 1 : 1. In Figure 1I, the powder diffractograms for two different reactant compositions and two milling times (4 h and 8 h) are shown. The reactions starting from the metal acetates led to the formation of products whose reflections are located in the middle between those of the pure fluoride references (Fig. 1Ia,b). This indicates, referring to Vegard's Law [29], that solid solutions with a cationic molar ratio of 1 : 1 are formed. No significant difference by variation of the milling time is noticeable except for a better signal to noise ratio, indicating a better crystallinity of the longer milled samples.

In case of $Ca(OH)_2$ and $PbCO_3$ as precursors, no traces of solid solutions can be detected. Instead, the pure binary fluorides are formed. Regarding the differences between the milling times, more α-PbF_2 is formed after 8 hours in comparison to the 4 hour reaction and CaF_2 seems to be in an amorphous state. ^{19}F MAS NMR spectra of the products of the reaction with metal acetates are given in Figure 2 I. As expected, five signals can be observed in the spectra.

In the fluorite structure the fluoride ion is tetrahedrally coordinated by four equivalent cations. If these four positions can be occupied by two different cations, five structural units

[FM_yPb_{4-y}] (with y = 0…4) are possible, each of it is giving a unique signal in the ^{19}F MAS NMR spectra. Therefore the five signals can be assigned to [FPb_4] at around -38 ppm up to [FCa_4] at -111 ppm. The shift to lower ppm values of the [FCa_4] signal could already be observed in $Ca_xSr_{1-x}F_2$ and similar systems [5, 17]. This can be explained by an increasing F-Ca bond length due to distortions in the structure. This behavior can be observed for all measured samples containing solid solutions in this study too. While the appearance of the five signals proves the formation of solid solutions, their intensity ratios are not always as expected. For a molar ratio of cations of 1 : 1 one would expect relative intensities of 6.25 %, 25 %, 37.5 %, 25 % and 6.25 % for [FPb_4], [FCa_1Pb_3], [FCa_2Pb_2], [FCa_3Pb_1] and [FCa_4], respectively. In our case units with only one cationic species are too dominant (Fig. 2II). So we can assume that CaF_2 and β-PbF_2 are formed in addition. Rotor-synchronized spin-echo spectra discover an additional ^{19}F signal at -120 ppm for the four hours reaction (Fig. 2Ic). This signal loses less intensity in the echo measurement compared to other signals. A similar signal was found in several of our reactions. We assume that it belongs to SiO_xF_y species from reactions of the fluorinating agent with the beaker material.

Regarding these promising results metal acetates as precursors were used in further experiments with different cationic molar ratios. In Figure 1II the X-ray powder diffractograms for three different molar ratios (x = 0.25, 0.5 and 0.75) are shown. In case of x = 0.75 and 0.5 the formation of solid solutions can be detected. Following Vegard's Law the reflections of the samples are shifted between the pure fluoride references accordingly. For x = 0.25, i.e. with high lead supply, no solid solutions can be detected by powder XRD measurements. Only the reflections of the β- and α-phase of PbF_2 are visible (Fig. 1IIc). CaF_2 has to be therefore in an amorphous state. Applying ^{19}F MAS NMR however (Fig. 2II), five signals for [FCa_yPb_{4-y}] can be detected for all three molar ratios. Hence, a $Ca_{0.25}Pb_{0.75}F_2$ solid solution is obviously formed, but it is apparently amorphous and therefore cannot be detected by XRD. The intensity patterns of the NMR spectra change along with the molar ratio. $Ca_{0.25}Pb_{0.75}F_2$ shows the more intense signals on the PbF_2 side of the spectra, $Ca_{0.75}Pb_{0.25}F_2$ shows more intense signals on the CaF_2 side. In all cases the signals of [FPb_4] and [FCa_4] are very prominent leading to the assumption that the pure binary fluorides, only confirmed by XRD for x = 0.25, are also formed during the reaction. Additionally, the signal positions for [FCa_yPb_{4-y}] were calculated by the superposition model [30,31] and were added as dotted lines to the spectra (parameters used are given in Table 2). They fit quite well to the experimental signal positions (Fig. 2IIa-c), but could be optimized by taking the relaxation of the M-F bond length through distortion of the structure into account. It was expected that the formation of

$Ca_xPb_{1-x}F_2$ is the most complicated one of the three studied systems. The difference between the ionic radii of Ca^{2+} and Pb^{2+} is quite large, comparable to Ca^{2+} and Ba^{2+}, which also did not allow the formation of $Ba_xCa_{1-x}F_2$ solid solutions over all molar ratios with the present preparation technique [17] involving ball milling the corresponding metal hydroxides with ammonium fluoride. Another hint is the rather complex phase diagram of CaF_2-PbF_2 calculated by Buchinskaya and Fedorov [32] which shows the formation of solid solutions only under certain conditions.

Synthesis of $Sr_xPb_{1-x}F_2$:

Analogous to the synthesis of $Ca_xPb_{1-x}F_2$, different metal precursors and milling times were tested. Again the metal acetates proved to be the optimal reactants for this reaction. Powder diffractograms for selected reactions (Sr : Pb; 1 : 1) are shown in Figure 3I. The samples prepared by metal acetates (Fig. 3Ia,b) show reflections in the middle between those of the references SrF_2 and PbF_2 following Vegard's Law [29] for both tested milling times. The reaction with the reactant mixture of $Sr(OH)_2$ and $PbCO_3$ did not lead to the formation of solid solutions. Instead, the pure fluorides besides non identified by-products are formed (Fig. 3Ic,d). In the ^{19}F MAS NMR spectra (Fig. 4I), for the reaction from acetates the five expected signals for $[FSr_yPb_{4-y}]$ at -36.0, -47.9, -61.0, -74.4 and -88.9 ppm can be observed. Additionally the $J_{F\text{-}Pb}$ coupling is visible on the signals belonging to mainly lead containing structural units. The coupling constant can be estimated as $J_{F\text{-}Pb}$ = 2.5 kHz which is in good agreement with the value found by us in PbF_2 prepared by milling [25]. A simulation of a spectrum for $Sr_{0.5}Pb_{0.5}F_2$ is shown in Figure 5a. For simulation purpose a more resolved spectrum (Fig. S1IIb) is used. The thick blue line represents the experimental spectrum. The thin lines are the fitted individual signals. The simulation shown here consists of 10 individual lines. Five singlets were fitted for the five $[FSr_yPb_{4-y}]$ units containing no NMR active ^{207}Pb species. The active nucleus ^{207}Pb has only a natural abundance of 22 %. So the units with no active Pb species are quite common, hence the dominant singlets. Then we fitted four doublets for $[FSr_y{}^{207}Pb_1Pb_{3-y}]$[1] at the same positions as the corresponding singlets. The triplets, quartets and quintets for $[FSr_y{}^{207}Pb_2Pb_{2-y}]$[1], $[FSr_y{}^{207}Pb_3Pb_{1-y}]$[1] and $[F^{207}Pb_4]$, respectively, were not fitted due to the low probability of occurrence and the resolution of the spectra, which is not high enough to show these signals. One additional line shows up at -84 ppm. This signal is assumed to belong to a Sr(OAc)F species. These M(OAc)F species are well known [33] and can sometimes be observed in other milling reactions starting from metal

[1] the total number of cations in one structural unit is always 4.

acetates [34]. Summing up all the individual fitted lines leads to the red line, which fits well compared to the original spectrum in blue. Only the *J*-couplings for the two lower field signals are not optimal caused by the asymmetric form of the original signal. Rotor-synchronized echo experiments (Fig. 4I c, d) do not add anything noteworthy except the different intensity loss of the signal at -84 ppm, indicating that this signal belongs to a species different to the solid solutions. Additional precursor combinations were successful only in case of $Sr_xPb_{1-x}F_2$. Using self-synthesized PbF_2 as described above and either (i) self-synthesized SrF_2 or (ii) $Sr(OAc)_2$ and NH_4F led to solid solutions as well, proven by XRD and MAS NMR (supporting information, Fig. SI-1). This is surprising, bearing in mind that usually milling pure fluorides together to obtain solid solutions is very time consuming, especially for the not stable $Ba_xCa_{1-x}F_2$ [16]. This indicates, that self-synthesizing the reactants either by milling or thermal treatment, activates them to get a faster access to the products. But it should be mentioned that these two reactions only work for $Sr_xPb_{1-x}F_2$, therefore, the ionic size difference might play the biggest role here.

The metal acetates were chosen for testing the reaction with different cationic molar ratios. The powder diffractograms of these samples (Fig. 3II) show the shift of the reflections between the references depending on the molar ratio, assuring the formation of the desired products. ^{19}F MAS NMR measurements (fig. 4II) confirm this further. The five signals, one for each $[FSr_yPb_{4-y}]$ unit, are clearly identifiable. Their positions are in good agreement to the calculated values obtained by using the superposition model [30]. There is a noticeable change of the intensity pattern depending on the cationic ratio. The spectrum of $Sr_{0.75}Pb_{0.25}F_2$ has more intense signals on the SrF_2 side, for $Sr_{0.25}Pb_{0.75}F_2$ it is the other way around. As for $Ca_xPb_{1-x}F_2$ the $[FSr_4]$ signals are more intense than expected, allowing the conclusion that the pure fluorides, although amorphous, are formed too. Also the shift of the ^{19}F signals of these units compared to SrF_2 (-88.9 vs. -88.0 ppm) and PbF_2 (-36.0 vs. -38.0 ppm) can be observed for the same reason as described above.

Synthesis of $Ba_xPb_{1-x}F_2$:

The difference between the ionic radii of Ba^{2+} and Pb^{2+} is larger than between Sr^{2+} and Pb^{2+} but smaller than between Ca^{2+} and Pb^{2+}. Therefore, the formation of solid solutions $Ba_xPb_{1-x}F_2$ can be expected. Again two different precursor mixtures will be described in detail. The powder diffractograms (Fig. 6I) show the reflections of the products from the reaction of the metal acetates and from the reaction of $Ba(OH)_2/PbCO_3$ (Ba: Pb; 1 : 1),

respectively, with NH_4F and with two different milling times. First of all it stands out, that the milling time had again not much influence on the qualitative outcome of the reaction. Solely the crystallinity of the samples is increased resulting in more intense reflections and a better signal to noise ratio. For the samples of the $Ba(OH)_2/PbCO_3$ reaction only reflections of PbF_2 and BaF_2 can be detected or they are at least just slightly shifted, indicating that just a small amount of the second cation is incorporated in the host lattices. In contrast, in case of the samples obtained from the acetate precursor mixture the reflections are directly in the middle between the references indicating the formation of $Ba_{0.5}Pb_{0.5}F_2$ solid solution. This is confirmed by ^{19}F MAS NMR measurements (Fig. 7I). Rotor-synchronized spectra demonstrate that the spin-spin relaxation is much faster for the mainly Pb-coordinated F-sites (Fig. 7Ic,d). However, all spectra are not well resolved, due to broad signals and a small ppm range ($\Delta(^{19}F)$[ppm](PbF_2-BaF_2): 24 ppm) in which the five signals for the five [FBa_yPb_{4-y}] units have to appear. To get more information the spectra were simulated with the help of the DMfit program (Fig. 5b). The blue line refers to the measured spectrum, the thin lines to the simulated individual signals. We needed 11 lines to obtain an optimal fit (red line). Five singlets were used for the five [FBa_yPb_{4-y}] units without F-Pb coupling. Their position was determined by calculations derived from the superposition model (parameters in Table 2) [30,31]. Four more doublets were added for the units with one F-^{207}Pb coupling comparable to the process for the simulation of $Sr_{0.5}Pb_{0.5}F_2$. Two more singlets were necessary to optimize the fit. One at around -8.0 ppm, which can be assigned to a Ba(OAc)F species [33,34] and one at -35 ppm, which might be an Pb(OAc)F species. While there is no clear evidence for the latter, a comparison can help: The ^{19}F signal of M(OAc)F species (M = Ca, Sr ,Ba) are shifted by 5 – 8 ppm compared to MF_2. When we assume the formation of Pb(OAc)F in our reaction, its ^{19}F chemical shift can be expected at about -35 ppm. The relative intensities of the signals are not fitting well compared to the expected values. The signal intensities belonging to the strontium richer units are too high. But as the simulation might not be perfect it shows that even a not well resolved spectrum with broad signals and a lot of overlapping signals can be simulated and can give an insight into the structure of the sample.

The reaction of the metal acetates was used for testing different cationic molar ratios. The results are given in Figure 6II (XRD) and Figure 7II (^{19}F MAS NMR). The powder diffractograms show that the obtained products follow Vegard's Law [29] closely. The shift of the reflections between those of the references is dependent on the molar ratio. For $Ba_{0.25}Pb_{0.75}F_2$ the signals on the PbF_2 side are more intense and vice versa for $Ba_{0.75}Pb_{0.25}F_2$. On a first view, the calculated signal positions for the [FBa_yPb_{4-y}] units, obtained from the

superposition model, do not fit very well (Fig. 7II). However, we can show with the simulation (Fig. 5b) that it is possible to fit the spectra with these calculated positions. It is obvious that the superposition of these signals causes maxima in the experimental spectrum which do not correspond to the isotropic chemical shift values.

Comparison of the three systems:

In Table 3 a summary of all syntheses carried out and their results are given. It is striking that the synthesis of $Sr_xPb_{1-x}F_2$ was possible with most of the precursor combinations. Most interestingly, even using one or even both metal precursors in form of the metal fluorides led to solid solutions at short milling times. The small size difference between the Sr^{2+} and the Pb^{2+} cationic radii might be the reason. The ^{19}F MAS NMR spectra of $Sr_xPb_{1-x}F_2$ showed the narrowest signals compared to the others. Even a scalar coupling $J_{F\text{-}Pb}$ can be observed and estimated. $Ba_xPb_{1-x}F_2$ can be synthesized with the second most precursor combinations. The radii difference is a bit larger than for Sr^{2+}/Pb^{2+}, hindering some more reactions to form solid solutions. The ^{19}F MAS NMR spectra are quite different in shape on a first view compared to $Sr_xPb_{1-x}F_2$. The signals are much broader and a scalar coupling cannot be resolved. The main reason for this is definitely the very small ppm range in which the five signals including their scalar coupling must appear. For $Ca_xPb_{1-x}F_2$ only the reaction of the two metal acetates led to the formation of the solid solution. The size difference of the cations might be too large. With higher lead content in the sample the formation of additional pure binary fluorides was increased. A similar behavior can also be observed for $Ba_xCa_{1-x}F_2$, where the cationic size difference is also quite high. Overall the metal acetates were proven to be the optimal precursors for all three systems. While not as reactive as the hydroxides and more reactive than the carbonates in this kind of reactions, it might be the good middle way to induce a reaction but to avoid the formation of the more favored pure fluorides. Using the usually more reactive NH_4HF_2 instead of NH_4F or increasing the milling time from 4 to 8 hours, showed no significant qualitative change in the reaction outcome. Only some of the samples were more crystalline, showing more intense reflections in XRD and more intense NMR signals.

Conductivity measurements

Additionally, DC conductivity measurements were carried out for these samples. The results are shown in Figure 8. The Arrhenius representation (Fig. 8I) gives an overview of the different conductivity values depending on the temperature and the cationic molar ratio. Three groups of lines can be identified: (i) the two lines with the lowest conductivity values belong

to $Ca(Sr)_{0.75}Pb_{0.25}F_2$; (ii) four lines with values of around one magnitude higher ($Ba_{0.75}Pb_{0.25}F_2$, $Ba(Sr)_{0.5}Pb_{0.5}F_2$ and self-prepared PbF_2); and (iii) another four lines again about one magnitude higher than the other ones before. These lines can be assigned to $Sr_{0.25}Pb_{0.75}F_2$, $Ba_{0.25}Pb_{0.75}F_2$, $Ca_{0.25}Pb_{0.75}F_2$ and $Ca_{0.5}Pb_{0.5}F_2$. The latter has to be regarded with care, because as stated before the sample is not phase pure. In general, two trends for the conductivity values can be observed:

(i) the higher the lead content the higher is the fluoride ion conductivity, and

(ii) the $Ba_xPb_{1-x}F_2$ system shows the highest values, followed by $Ca_xPb_{1-x}F_2$ and $Sr_xPb_{1-x}F_2$.

All of them are by few magnitudes higher than the one measured by us for $Ca_xSr_{1-x}F_2$ and $Ba_xSr_{1-x}F_2$ and even higher than those for the pure alkaline earth metal fluorides. Figure 8II (left-hand ordinate) shows a comparison of the conductivities dependent on the cationic molar ratio. The maximum is shifted towards $M_{0.25}Pb_{0.75}F_2$ (M = Ca, Sr, Ba) as compared to the alkaline earth metal systems, showing the maximum at around x = 0.5. The activation energy E_A (right-hand ordinate) is directly related to the conductivity. The higher the conductivity the lower is E_A. Thus, it is no surprise, that the E_A values are lower than for the $M^a_xM^b_{1-x}F_2$ (M = Ca, Sr, Ba) solid solutions.

Conclusions

The present study demonstrates the possibility of synthesizing $M_xPb_{1-x}F_2$ (M = Ca, Sr, Ba) solid solutions by high-energy ball milling. For all three alkaline earth metal cations the metal acetates and ammonium fluoride are proven to be the optimal precursor combination for this reaction. While for $Sr_xPb_{1-x}F_2$ and $Ba_xPb_{1-x}F_2$ the mutual substitution of cations on their lattice positions occurs for all tested molar ratios, $Ca_xPb_{1-x}F_2$ shows this behavior only for x > 0.25. Here the pure fluorides are formed instead. As long as the products are crystalline, XRD measurements allow a quick confirmation of success of synthesis due to the reflections following Vegard's Law. ^{19}F MAS NMR spectra of samples reveal the five signals, including $J_{F\text{-}Pb}$ coupling, belonging to the $[FM_yPb_{4-y}]$ local structural units, underlining the formation of solid solutions. The ^{19}F chemical shifts of these units were calculated and compared using the superposition model by Bureau *et al.* [30]. Simulations of the NMR spectra further showed, that the samples are not phase pure. Signals belonging to the pure binary fluorides and presumably M(OAc)F species are detected. A mixing effect for the ionic conductivity could

be proven by impedance spectroscopy measurements. The conductivity values are by several magnitudes higher than those of the pure fluorides and are also increased in comparison to the already investigated $M^a_xM^b_{1-x}F_2$ (M = Ca, Sr, Ba) solid solutions. Therefore, the presented synthesis route can be extended on more cations than the alkaline earth metal ones and may prove an easy and fast access to prepare fast fluoride ion conductors.

Acknowledgements

The authors thank the research training network GRK 1582/2 “Fluorine as a Key Element” of DFG (Deutsche Forschungsgemeinschaft) for financial support. Paul Heitjans is supported by a Niedersachsen Professorship.

References

[1] A. Düvel, J. Bednarcik, V. Šepelák, P. Heitjans, *J. Phys. Chem. C* **2014**, *118*, 7117–7129.

[2] C. Rongeat, M. A. Reddy, R. Witter, M. Fichtner, **2014**, *ACS Applied Materials and Interfaces*, 2103-2110.

[3] C. Rongeat, M. A. Reddy, R. Witter, M. Fichtner, *J. Phys. Chem. C* **2013**, *117*, 4943–4950.

[4] H. Bhatia, T. Thieu, A. Pohl, V. S. K. Chakravadhanula, M. Fawey, C. Kübel, M. Fichtner, *ACS Appl. Mater. Interfaces* **2017**, *9*, 23707–23715.

[5] A. Düvel, P. Heitjans, P. Fedorov, G. Scholz, G. Cibin, A. V. Chadwick, D. M. Pickup, S. Ramos, L. W. L. Sayle, E. K. Sayle, et al., *J. Am. Chem. Soc.* **2017**, *139*, 5842–5848.

[6] W. Li, Z. Liu, Z. Zhou, J. Song, B. Mei, L. Su, *J. Eur. Ceram. Soc.* **2016**, *36*, 3481–3486.

[7] F. Wang, X. Liu, *Chem. Soc. Rev.* **2009**, *38*, 976.

[8] M. Haase, H. Schäfer, *Angew. Chemie - Int. Ed.* **2011**, *50*, 5808–5829.

[9] I. N. Ogorodnikov, V. A. Pustovarov, S. I. Omelkov, L. I. Isaenko, A. P. Yelisseyev, A. A. Goloshumova, S. I. Lobanov, *J. Lumin.* **2014**, *145*, 872–879.

[10] B. Ritter, P. Haida, T. Krahl, G. Scholz, E. Kemnitz, *J. Mater. Chem. C* **2017**, *5*, 5444–5450.

[11] B. Ritter, P. Haida, F. Fink, T. Krahl, K. Gawlitza, K. Rurack, G. Scholz, E. Kemnitz,

Dalt. Trans. **2017**, *46*, 2925–2936.

[12] V. V Boldyrev, *Proc. Indian natn. Sci. Acad.* **1986**, *52A*, 400 417.

[13] J.-L. Do, T. Friščić, *ACS Cent. Sci.* **2016**, *3*, 13–19.

[14] P. Baláž, M. Achimovičová, M. Baláž, P. Billik, Z. Cherkezova-Zheleva, J. M. Criado, F. Delogu, E. Dutková, E. Gaffet, F. J. Gotor, et al., *Chem. Soc. Rev.* **2013**, *42*, 7571–637.

[15] S. Kipp, V. Šepelák, K. D. Becker, *Chemie unserer Zeit* **2005**, *39*, 384–392.

[16] A. Düvel, B. Ruprecht, P. Heitjans, M. Wilkening, *J. Phys. Chem. C* **2011**, *115*, 23784–23789.

[17] M. Heise, G. Scholz, A. Düvel, P. Heitjans, E. Kemnitz, *Solid State Sci.* **2016**, *60*, 65–74.

[18] M. Uno, M. Onitsuka, Y. Ito, S. Yoshikado, *Solid State Ionics* **2005**, *176*, 2493–2498.

[19] L. Batzdorf, F. Fischer, M. Wilke, K.-J. Wenzel, F. Emmerling, *Angew. Chemie Int. Ed.* **2015**, *54*, 1799–1802.

[20] F. Fischer, N. Fendel, S. Greiser, K. Rademann, F. Emmerling, *Org. Process Res. Dev.* **2017**, *21*, 655-659.

[21] D. E. Crawford, J. Casaban, *Adv. Mater.* **2016**, 5747–5754.

[22] M. Dreger, G. Scholz, E. Kemnitz, *Solid State Sci.* **2012**, *14*, 528–534.

[23] G. Scholz, K. Meyer, A. Düvel, P. Heitjans, E. Kemnitz, *Zeitschrift fur Anorg. und Allg. Chemie* **2013**, *639*, 960–966.

[24] M. A. Subirana-Manzanares, M. Sanchez-Sala, J. Pons, C. Domingo, J. A. Ayllón, *Mater. Lett.* **2016**, *163*, 76–80.

[25] M. Heise, G. Scholz, E. Kemnitz, *Solid State Sci.* **2017**, *72*, 41-46.

[26] JCPDS-ICDD, International Centre for Diffraction Data: PDF-2 Database (Sets 1e51 plus 70e89). PA 19073-3273 USA, Release 2001 e PCPDFWIN Version 2.2.

[27] D. G. Cory, W. M. Ritchey, *J. Magn. Reson.* **1988**, *80*, 128–132.

[28] D. Massiot, F. Fayon, M. Capron, I. King, S. Le Calvé, B. Alonso, J. O. Durand, B. Bujoli, Z. Gan, G. Hoatson, *Magn. Reson. Chem.* **2002**, *40*, 70–76.

[29] L. Vegard, *Z. Phys.* **1921**, *5*, 17–26.

[30] B. Bureau, G. Silly, J. Y. Buzaré, J. Emery, *Chem. Phys.* **1999**, *249*, 89–104.

[31] G. Scholz, S. Breitfeld, T. Krahl, a. Düvel, P. Heitjans, E. Kemnitz, *Solid State Sci.* **2015**, *50*, 32–41.

[32] I. I. Buchinskaya, P. P. Fedorov, *Russ. Chem. Rev.* **2004**, *73*, 371–400.

[33] L. Schmidt, "Synthese und Charakterisierung von Nano-SrF2 und -YbF3 für Anwendungen in der Dentalmedizin", Dissertation, Humboldt-Universtät zu Berlin, **2015**.

[34] S. Breitfeld, G. Scholz, E. Kemnitz, **2017**, *in preparatiom* .

Figure captions

Scheme 1. General scheme for the synthesis of $M_xPb_{1-x}F_2$.
(R: OH^-, OAc^-; ½ CO_3^{2-}, F^- / M = Ca, Sr, Ba)

Figure 1.

I. XRD patterns of "$Ca_{0.5}Pb_{0.5}F_2$" samples (formal composition based on the molar ratio of the used metal precursors) synthesized by milling NH_4F with: $Pb(OAc)_2 \cdot 3\ H_2O$ and $Ca(OAc)_2 \cdot H_2O$ for a) 4 h, b) 8 h; $Ca(OH)_2$ and $PbCO_3$ for c) 4 h, and d) 8 h.

II. XRD patterns of $Ca_xPb_{1-x}F_2$ samples synthesized by milling $Pb(OAc)_2 \cdot 3\ H_2O$, $Ca(OAc)_2 \cdot H_2O$ and NH_4F for 8 h with different molar ratios: a) x = 0.75; b) x = 0.5; c) x = 0.25.

Reference: dotted lines: reflection positions of β-PbF_2 (PDF chart: 6-251); dashed line: reflection positions of CaF_2 (PDF chart: 35-816).

Figure 2.

I. ^{19}F MAS NMR spectra of $Ca_{0.5}Pb_{0.5}F_2$ samples synthesized by milling $Pb(OAc)_2 \cdot 3\ H_2O$, $Ca(OAc)_2 \cdot H_2O$ and NH_4F:
single pulse spectra: a) 4 h milling, b) 8 h milling;
rotor synchronized spin echo spectra (dipolar evolution time: 0.5 ms): c) 4 h milling; d) 8 h milling.

II. ^{19}F MAS NMR single pulse spectra of $Ca_xPb_{1-x}F_2$ samples synthesized by milling $Pb(OAc)_2 \cdot 3\ H_2O$, $Ca(OAc)_2 \cdot H_2O$ and NH_4F for 8 h: a) x = 0.75; b) x = 0.5; c) x = 0.25. The dotted lines represent calculated positions of the five possible structural units $[FPb_{4-x}M_x]$ using the superposition model from Bureau *et al.* [30,31].

Figure 3.

I. XRD patterns of "$Sr_{0.5}Pb_{0.5}F_2$" samples synthesized by milling NH_4F with:
$Pb(OAc)_2 \cdot 3\ H_2O$ and $Sr(OAc)_2$ for a) 4 h and b) 8 h;
$Sr(OH)_2$ and $PbCO_3$ for c) 4 h and d) 8 h.

II. XRD patterns of $Sr_xPb_{1-x}F_2$ samples synthesized by milling $Pb(OAc)_2 \cdot 3\ H_2O$, $Sr(OAc)_2$ and NH_4F for 8 h with different molar ratios: a) x = 0.75; b) x = 0.5; c) x = 0.25.

Reference: dotted lines: reflection positions of β-PbF_2 (PDF chart: 6-251); dashed line: reflection positions of SrF_2 (PDF chart: 6-262).

Figure 4.

I. ^{19}F MAS NMR spectra of $Sr_{0.5}Pb_{0.5}F_2$ samples synthesized by milling $Pb(OAc)_2 \cdot 3\ H_2O$, $Sr(OAc)_2$ and NH_4F:
single pulse spectra: a) 4 h milling, b) 8 h milling;
rotor synchronized spin echo spectra (dipolar evolution time: 0.5 ms): c) 4 h milling; d) 8 h milling.

II. ^{19}F MAS NMR single pulse spectra of $Sr_xPb_{1-x}F_2$ samples synthesized by milling $Pb(OAc)_2 \cdot 3\ H_2O$, $Sr(OAc)_2$ and NH_4F for 8 h; with a) x = 0.75; b) x = 0.5; c) x = 0.25. The dotted lines represent the calculated positions of the five possible structural units $[FPb_{4-x}M_x]$ using the superposition model from Bureau *et al*. [30,31].

Figure 5.

Simulations of ^{19}F MAS NMR spectra of a) $Sr_{0.5}Pb_{0.5}F_2$ and b) $Ba_{0.5}Pb_{0.5}F_2$ using the DMfit program [28]. The blue lines are the measured spectra, the red lines represent the superposition of the simulated signal contributions. Thin lines belong to simulated signals of the five structural units $[FM_xPb_{4-x}]$, the doublet signals are due to the present scalar $J_{F\text{-}Pb}$ coupling (J = 2.5 kHz) and additional small signals (see text) are used to optimize the fit.

Figure 6.

I. XRD patterns of "$Ba_{0.5}Pb_{0.5}F_2$" samples synthesized by milling NH_4F with: $Pb(OAc)_2 \cdot 3\ H_2O$ and $Ba(OAc)_2$ for a) 4 h and b) 8 h; $Ba(OH)_2$ and $PbCO_3$ for c) 4 h and d) 8 h.

II. XRD patterns of $Ba_xPb_{1-x}F_2$ samples synthesized by milling $Pb(OAc)_2 \cdot 3\ H_2O$, $Ba(OAc)_2$ and NH_4F for 8 h with different molar ratios: a) x = 0.75; b) x = 0.5; c) x = 0.25.

Reference: dotted line: reflection positions of β-PbF_2 (PDF chart: 6-251); dashed line: reflection positions of BaF_2 (PDF chart: 4-452)

Figure 7.

I. ^{19}F MAS NMR spectra of $Ba_{0.5}Pb_{0.5}F_2$ samples synthesized by milling $Pb(OAc)_2 \cdot 3\ H_2O$, $Ba(OAc)_2$ and NH_4F:
single pulse spectra: a) 4 h milling, b) 8 h milling;
rotor synchronized spin echo spectra (dipolar evolution time: 0.5 ms): c)4 h milling; d) 8 h milling.

II. ^{19}F MAS NMR single pulse spectra of $Ba_xPb_{1-x}F_2$ samples synthesized by milling $Pb(OAc)_2 \cdot 3\ H_2O$, $Ba(OAc)_2$ and NH_4F for 8 h; with a) x = 0.75; b) x = 0.5; c) x = 0.25. The dotted lines represent the calculated position of the five possible structural units $[FPb_{4-x}M_x]$ using the superposition model from Bureau *et al*. [30, 31].

Figure 8.

I. Arrhenius plot of the DC conductivities of $M_xPb_{1-x}F_2$ samples prepared with three different cation ratios by milling the corresponding metal acetates with NH_4F for 8 hours and PbF_2. The latter was prepared in advance by milling of $Pb(OAc)_2 \cdot 3\ H_2O$ with NH_4F for 4 hours.

II. Variation of the DC conductivity determined at 220 °C as well of the activation energy E_a dependent on the cation ratio in $M_xPb_{1-x}F_2$. The samples were prepared as described in the caption to Fig. 7I.

Figure SI-1.

I. XRD patterns of $Sr_{0.5}Pb_{0.5}F_2$ samples synthesized by milling NH_4F with: a) PbF_2 prepared by thermal synthesis and $Sr(OAc)_2$ for 4 h; b) PbF_2, prepared by thermal synthesis, SrF_2, prepared by milling of $Sr(OH)_2$ and NH_4F, for 4 h.
Reference: dotted line: β-PbF_2 (PDF chart: 6-251); dashed line: SrF_2 (PDF chart: 6-262)

II. ^{19}F MAS NMR spectra (a, c) and rotor synchronized spin echo spectra (b, d; dipolar evolution time: 0.5 ms) of $Sr_{0.5}Pb_{0.5}F_2$ samples synthesized by milling: (a, b) PbF_2, $Sr(OAc)_2$ and NH_4F; and (c, d) PbF_2 and SrF_2.

Tables

Table 1. Chemicals used in the present study.

Compound	Origin	Purity	PDF number [26]
$Pb(OAc)_2 \cdot 3\ H_2O$	Sigma-Aldrich	≥ 99 %	14-829
$PbCO_3$	Sigma-Aldrich	≥ 99 %	70-2052
PbF_2	self-prepared	---	6-251 (β-phase)
$Ca(OAc)_2 \cdot H_2O$	Sigma-Aldrich	> 99 %	14-780
$Ca(OH)_2$	Sigma-Aldrich	> 96 %	44-1481
CaF_2	self-prepared	---	35-816
$Sr(OAc)_2$	Sigma-Aldrich	unspecified	37-655
$Sr(OH)_2$	Sigma-Aldrich	95 %	27-847
SrF_2	self-prepared	---	6-262
$Ba(OAc)_2$	Sigma-Aldrich	99 %	26-131
$Ba(OH)_2$	Sigma-Aldrich	95 %	44-585
BaF_2	self-prepared	---	4-452
NH_4F	Sigma-Aldrich	≥ 98 %	35-758

Table 2. **Parameters used for the calculation of the signal positions with the superposition model [30, 31].**

Parameter	d_0 in [Å]	d in [Å]	α_0	σ_0
Ca^{2+}	2.364	2.364	2.976	-46.3
Sr^{2+}	2.511	2.511	2.856	-51.4
Ba^{2+}	2.685	2.685	3.256	-70.0
Pb^{2+}	2.57	2.57	2.880	-64.0

Table 3. Overview about experiments performed with different precursor compounds and the obtained products (The M : Pb ratio was adjusted as 1 : 1)*.

Alkaline earth metal precursor	Lead precursor	Calcium	Strontium	Barium
$M(OAc)_2$	$Pb(OAc)_2$	✓	✓	✓
$M(OH)_2$	$Pb(OAc)_2$	–	✓	✓
$M(OAc)_2$	$PbCO_3$	(✓)	(✓)	–
$M(OH)_2$	$PbCO_3$	(✓)	(✓)	–
MF_2	$Pb(OAc)_2$	–	–	–
MF_2	$PbCO_3$	(✓)	–	–
$M(OAc)_2$	PbF_2	–	✓	✓
$M(OH)_2$	PbF_2	(✓)	✓	–
$M(OAc)_2$	PbF_2 without NH_4F	–	–	–
$M(OH)_2$	PbF_2 without NH_4F	–	–	–
MF_2	PbF_2	(✓)	✓	(✓)

* ✓: solid solutions are the main product; (✓): solid solutions are formed beside other products; –: solid solutions could not be detected.

Figure 1.

I

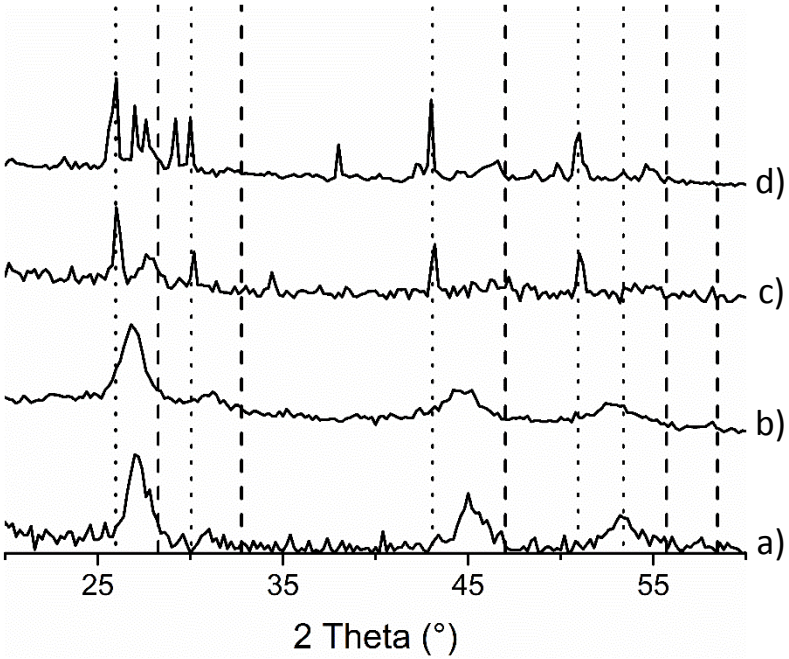

II

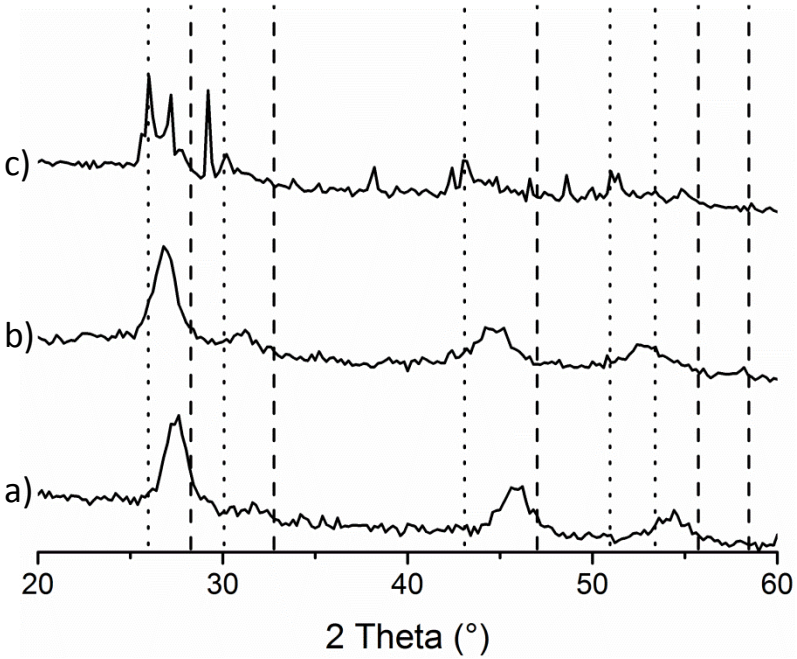

Figure 2.

I

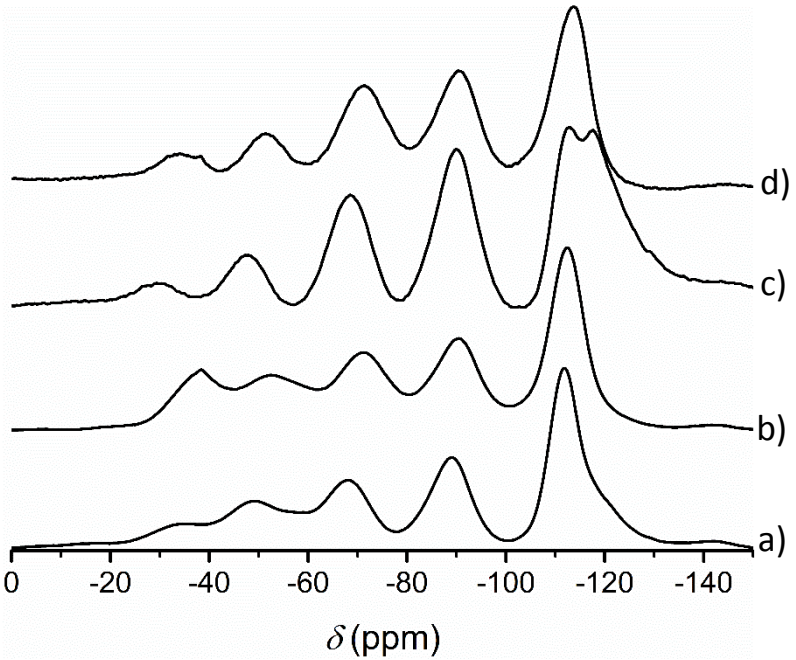
d)
c)
b)
a)
0
-20
-40
-60
-80
-100
-120
-140
δ (ppm)

II

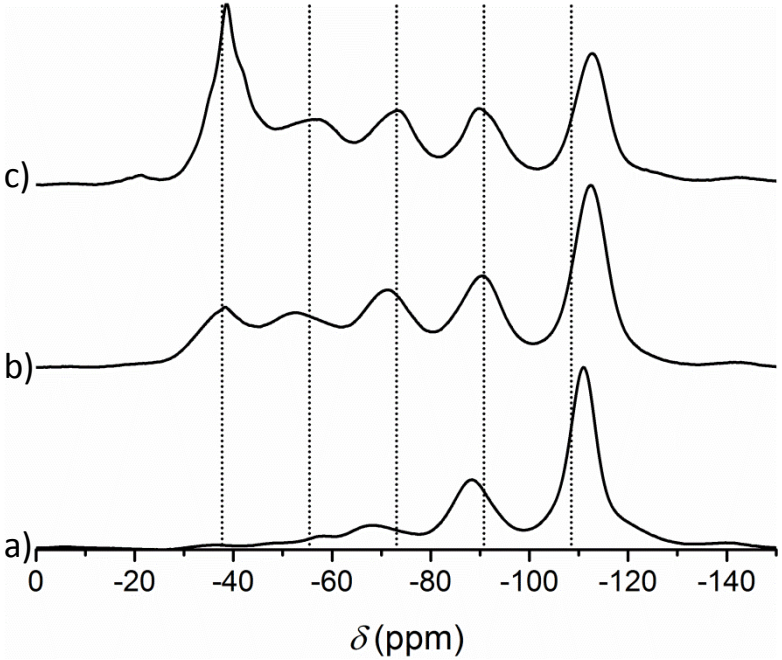
c)
b)
a)
0
-20
-40
-60
-80
-100
-120
-140
δ (ppm)

Figure 3.

I

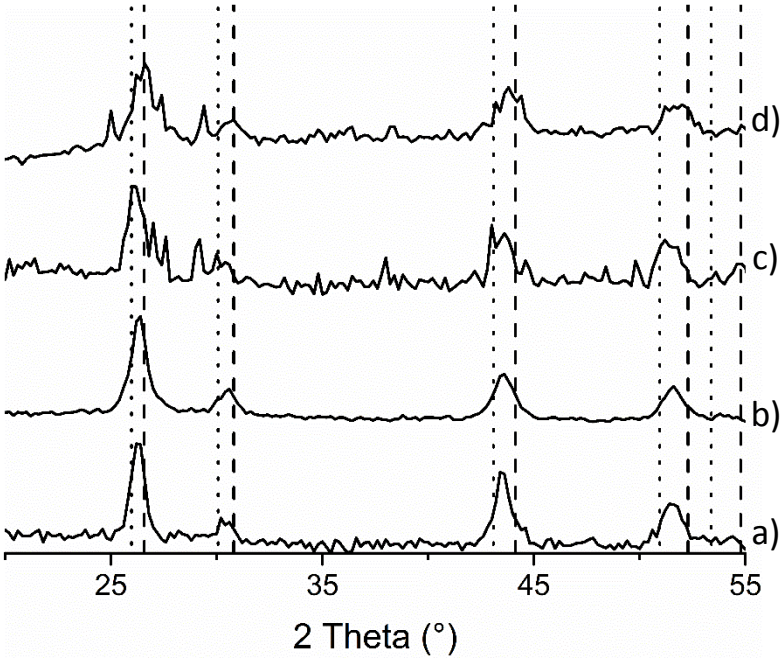

II

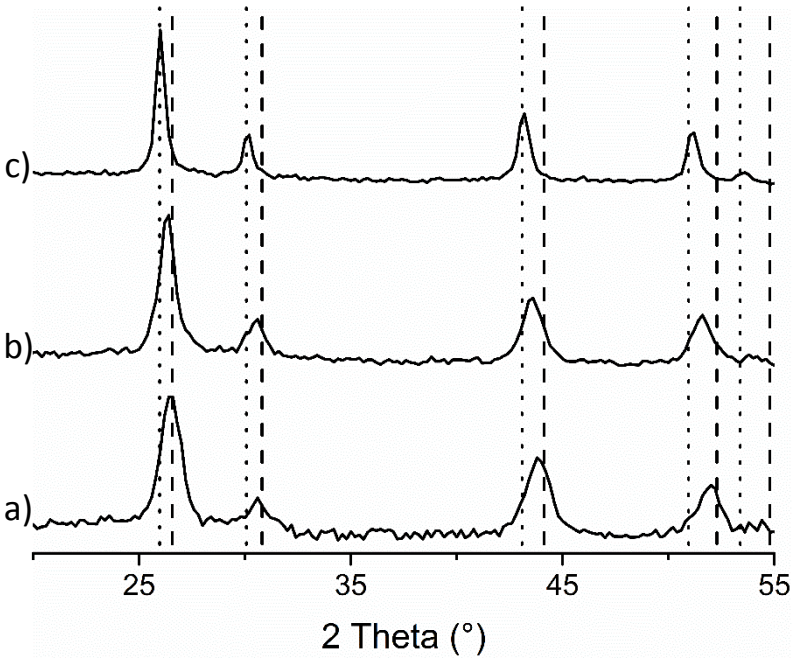

Figure 4.

I

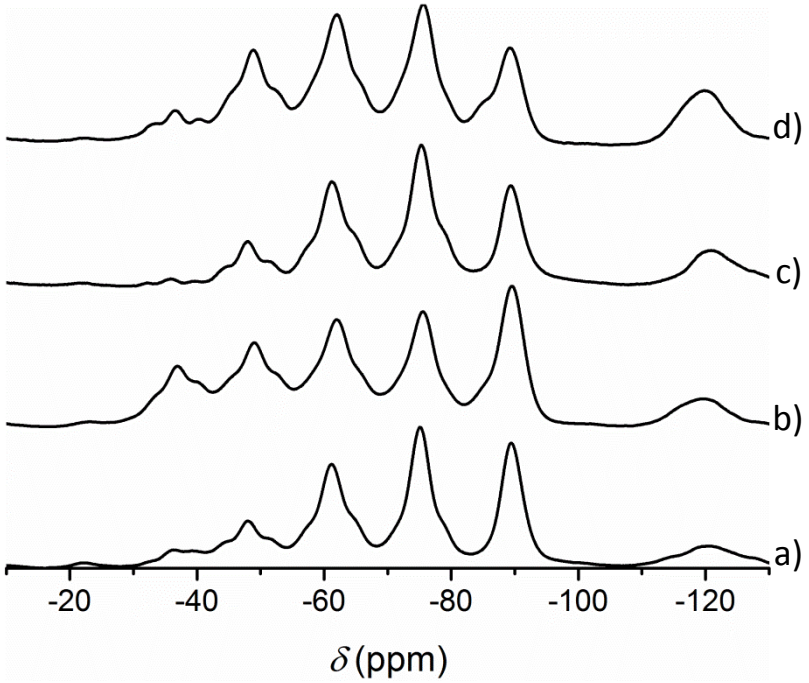

II

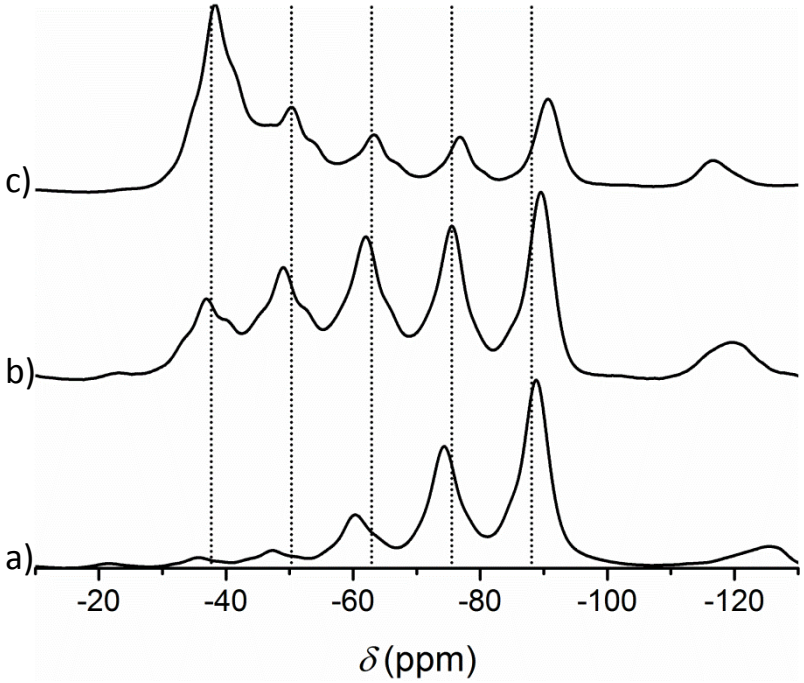

Figure 5.

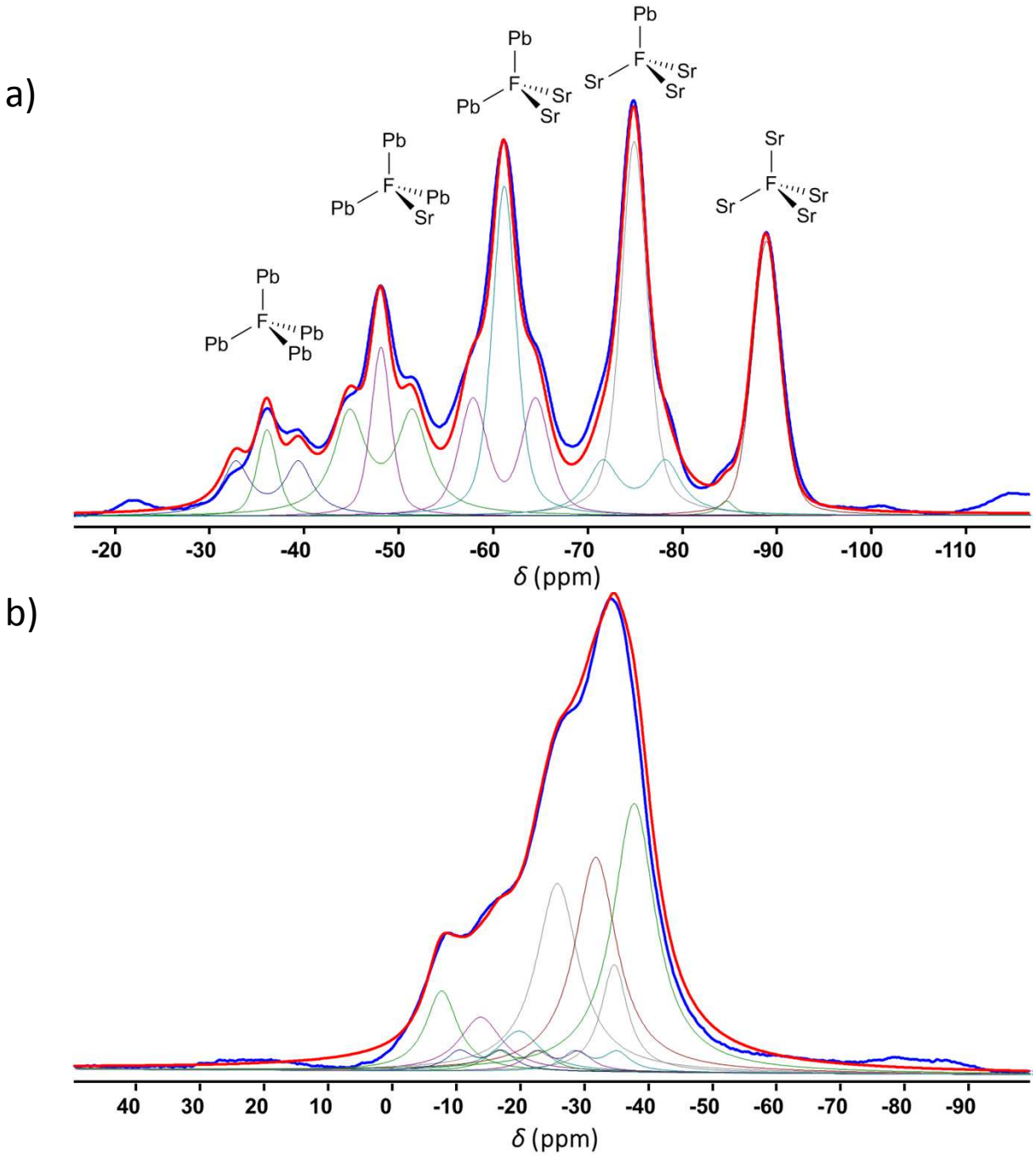
a)
Pb
F
Pb
Pb
Sr
Sr
Pb
F
Pb
Sr
Sr
Pb
F
Sr
Sr
Sr
Pb
F
Pb
Pb
Pb
Sr
F
Sr
Sr
Sr
-20
-30
-40
-50
-60
-70
-80
-90
-100
-110
δ (ppm)
b)
40
30
20
10
0
-10
-20
-30
-40
-50
-60
-70
-80
-90
δ (ppm)

Figure 6.

I

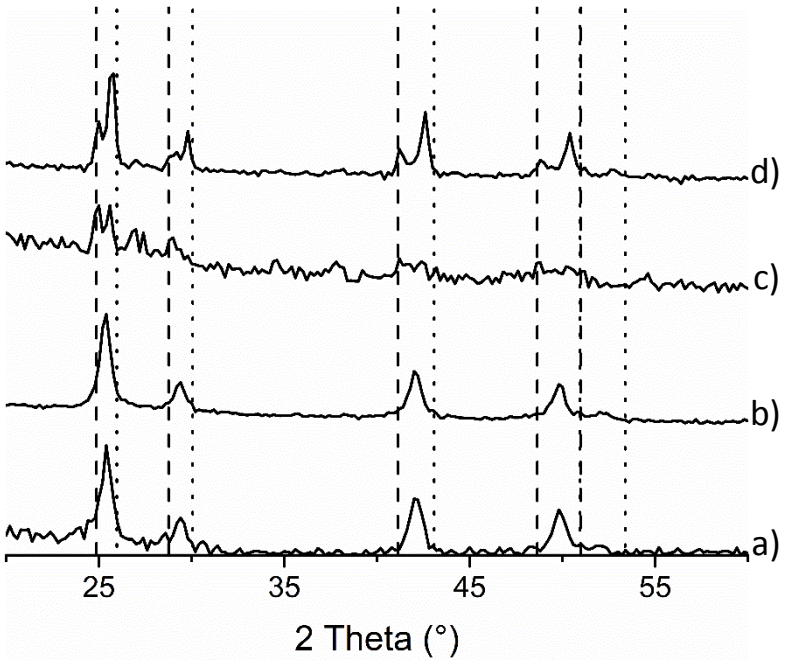

II

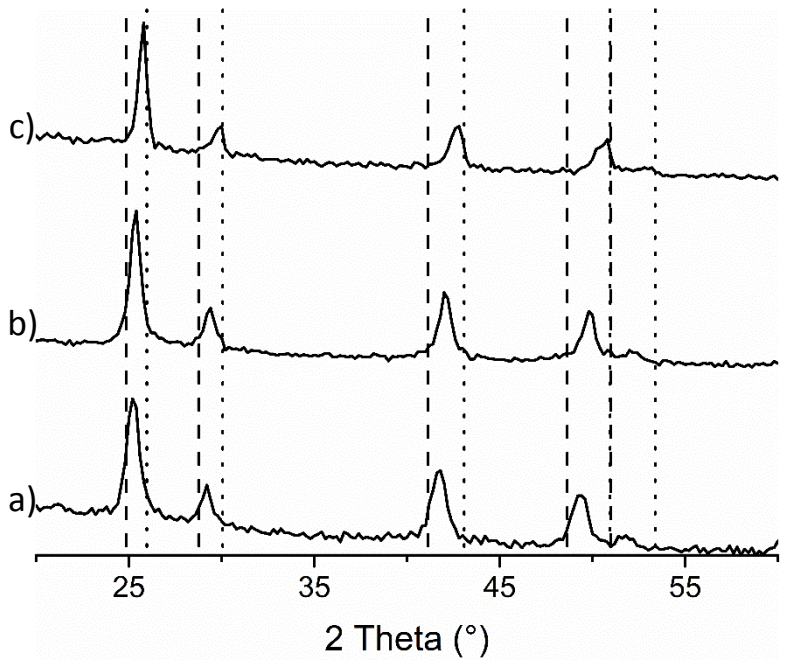

Figure 7.

I

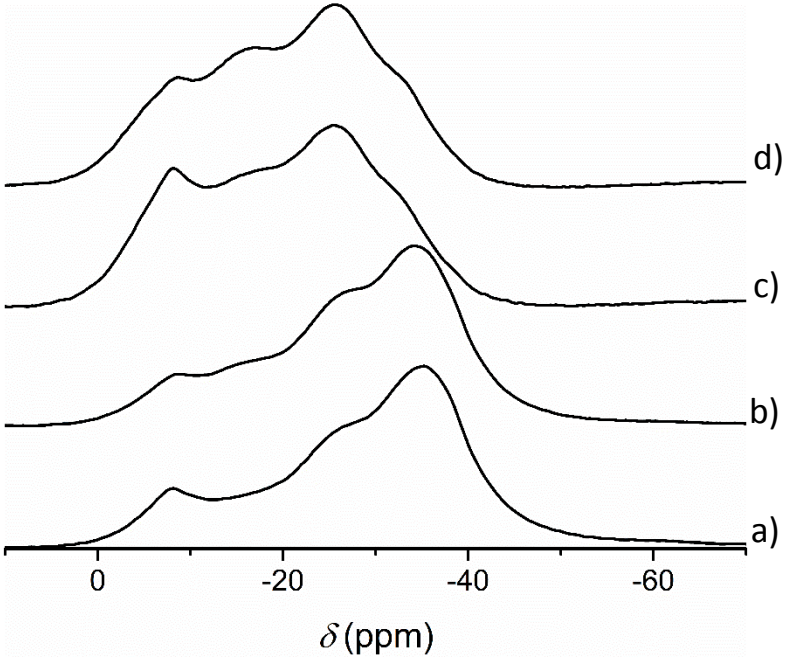

II

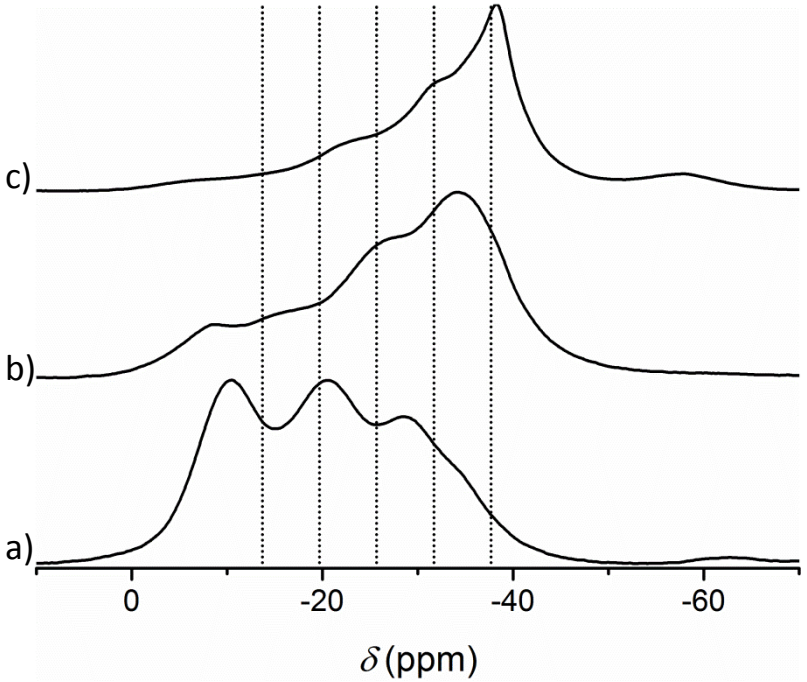

Figure 8I.

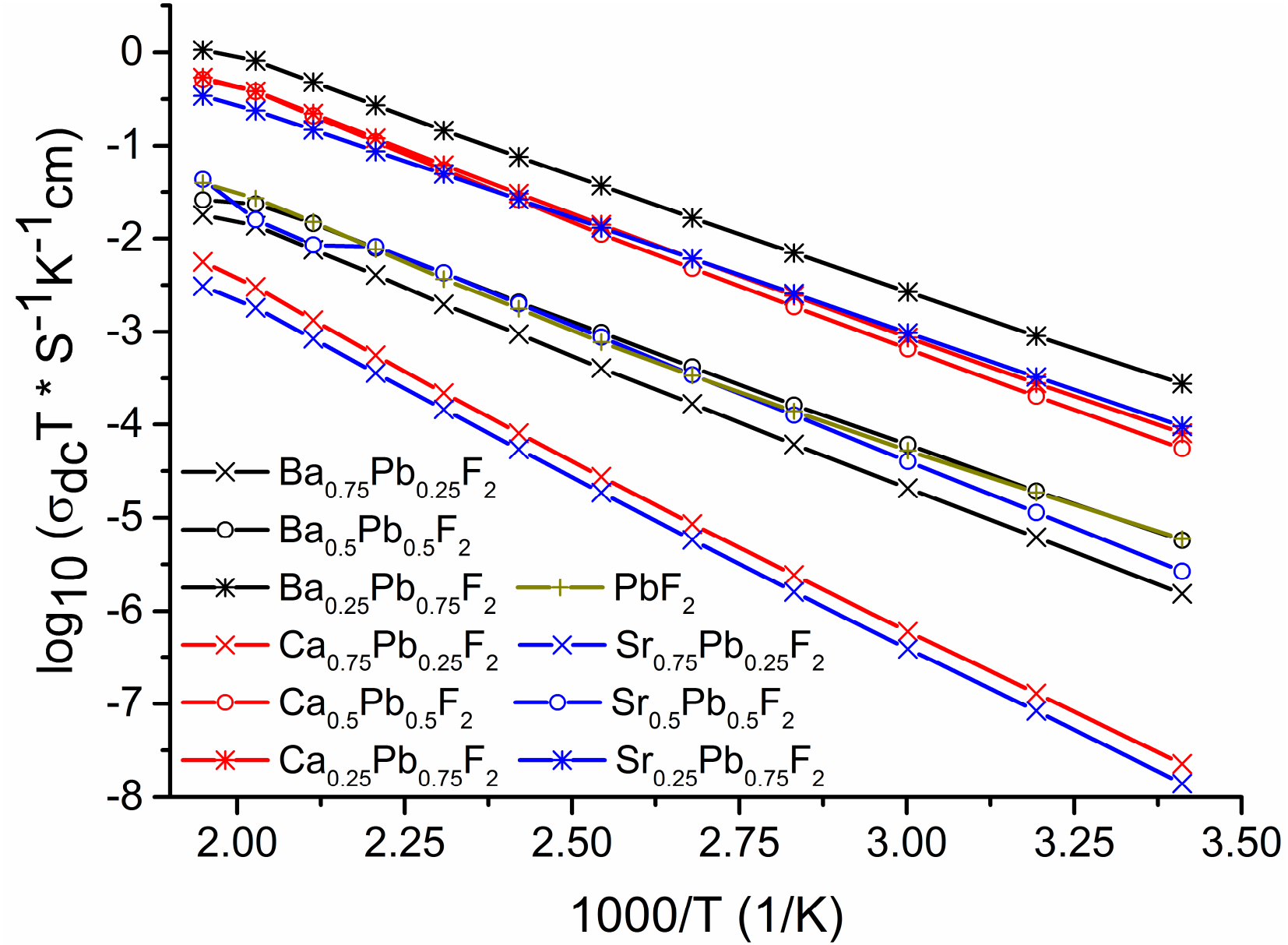

Figure 8II.

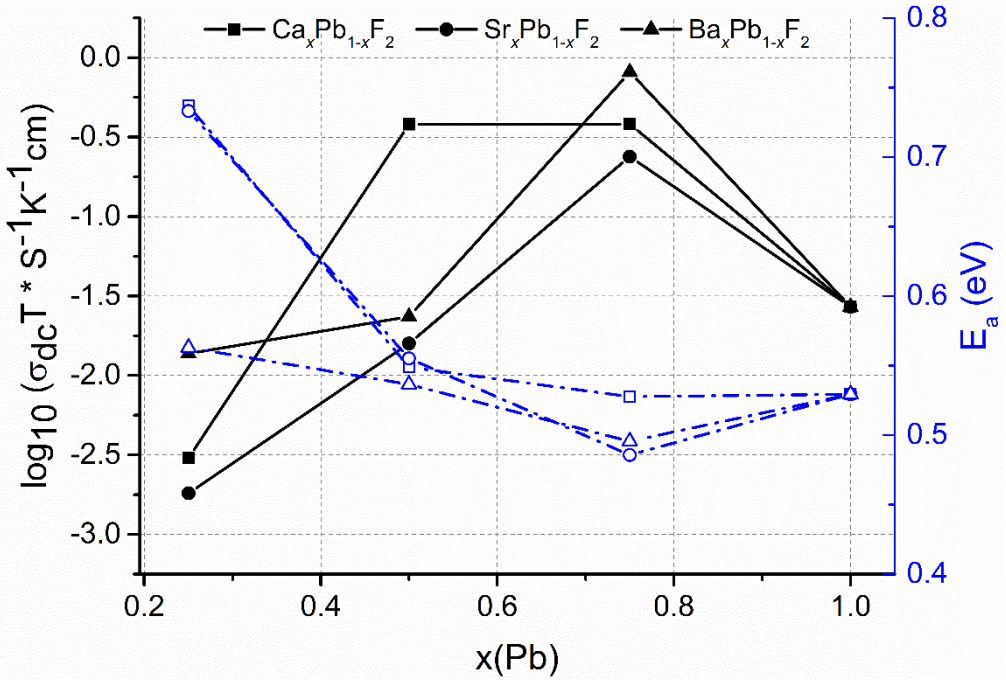

Figure SI-1.

I

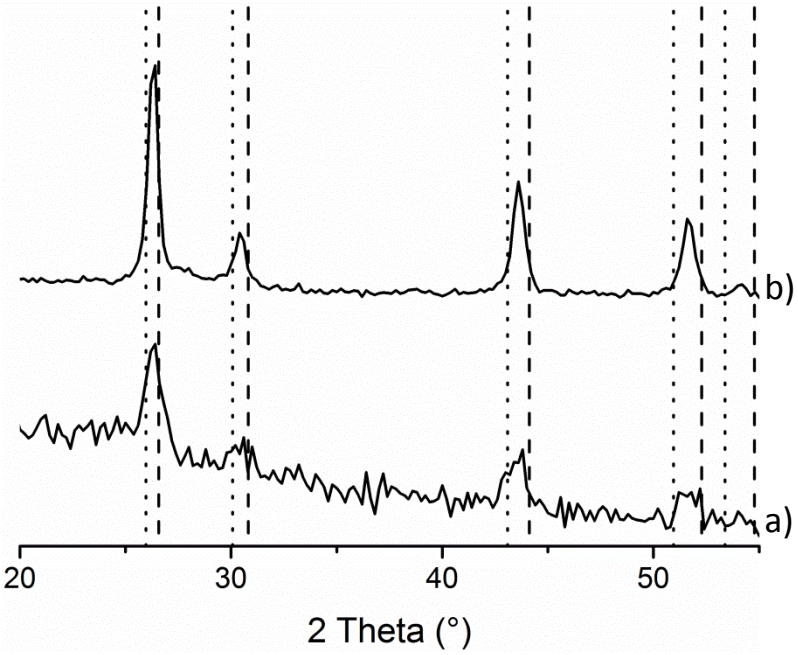

II

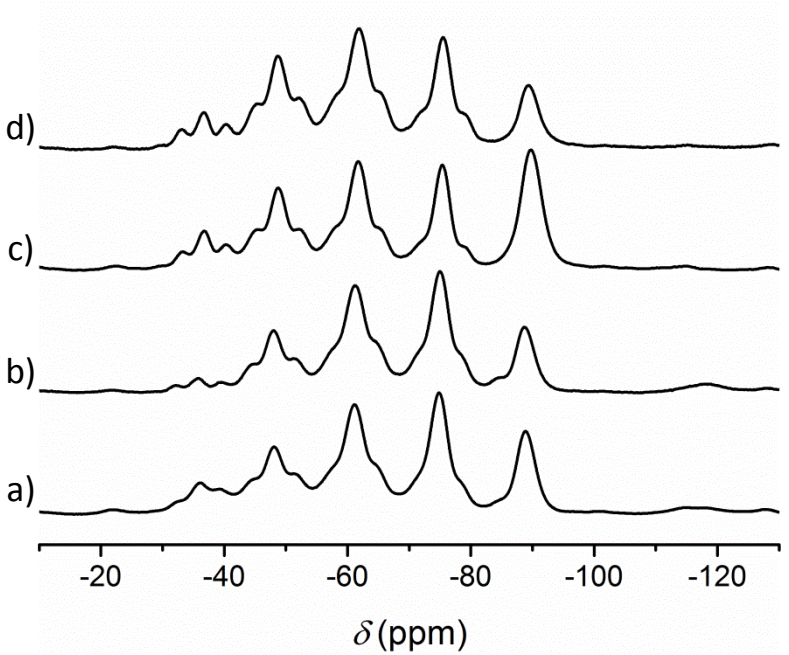

Scheme 1

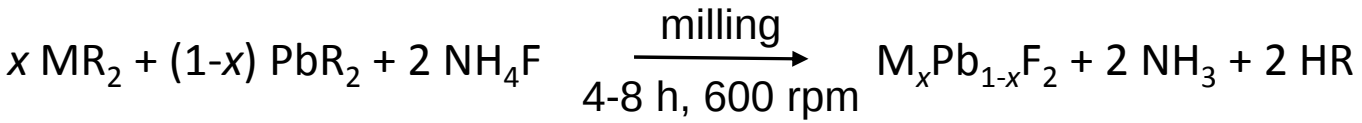

Highlights

- Mechanochemical synthesis of $M_xPb_{1-x}F_2$ with different precursors
- Structural information was obtained by ^{19}F MAS NMR spectroscopy and XRD measurements
- Simulation of NMR spectra
- The temperature dependent DC conductivity was determined